



ÉCOLE DES MINES DE SAINT-ÉTIENNE

PROTOTYPING PROJECT DESIGN REPORT

Capacitive force sensor

Students:

Faiz MOHAMMAD

Vincent LALANNE

Table des matières

1	Introduction	2
2	Weight measurement methods	3
2.1	Weighing under the cab floor	3
2.2	Weighing at the suspension rope	3
2.2.1	Measurement by two electrodes around the cable	3
2.2.2	Measurement by parallel plane electrodes	4
3	Physical modelling	5
3.1	Sizing ribs	5
3.2	Mathematical modelling	7
3.3	3D modelling	8
4	Experimental results	11
4.1	Conditioner circuit design	11
4.2	Tensile test	17
4.3	Creep test	20
4.4	Relaxation test	22
5	Analysis of results	22
6	Improvement ideas	23
7	Synthesis	25

1 Introduction

With the ever-increasing quest to save time and effort, the presence of lifts in modern buildings has become a matter of course [1]. There are over 15 million lifts in the world, some of which are used several hundred times a day. They must therefore comply with strict safety constraints. For example, if the maximum authorised weight in the cabin is exceeded, a safety system is often triggered to prevent the cabin from moving or to lower it safely to the nearest level. There are a number of overload detection systems available, produced by companies such as Zemic, Kone and Otis. This report will detail the design reasoning followed in order to produce a functional prototype of a capacitive force sensor using deformation of a test body. The problem that this report aims to address is that of the coherence of the choice of a capacitive force sensor to measure a load of the order of three tonnes with a maximum measurement error of around ten kilograms and a resolution of one kilogram.

The challenge is to design a system that avoids overloading the cabin as much as possible, so that the lift does not have to be blocked. One possible solution is to be able to control the lift in "load" or "unload" mode. The "load" mode corresponds to normal use of the lift, where the lift optimises each journey to make as few return trips as possible. The "unload" mode prohibits the lift from taking on new users, and directs the lift first to the floors requested by users already inside the cabin. The switch from one mode to the other is determined by the total weight inside the cabin. If this weight reaches or exceeds 90

This would enable journeys to be better optimised, in that the risk of overloading, and therefore of stalling, is avoided. Similarly, the situation where the lift stops to pick up a user on a floor but is too full for them to get on is avoided. This ensures just-in-time operation, avoids wasting users' time, and saves unnecessary journeys. The problem, then, is to design a system capable of weighing the cab and making the decisions that follow.

In this report, only the 'weight measurement' part (or, alternatively, 'force measurement') will be covered. The challenge is to design a sensor that is sufficiently accurate to be able to engage the right mode at the right time, and sufficiently robust to withstand the weight of the lift and its users over time. Several types of sensor are possible in this application, including strain gauge sensors and hydraulic sensors. In this study, we chose a capacitive sensor.

2 Weight measurement methods

2.1 Weighing under the cab floor

A first solution considered was to install a plate under the floor of the cab, in order to obtain a system similar to a bathroom scale. This would have enabled accurate weight measurement, but proved difficult to install. If a user were to stand in a corner of the cab, the weight measurement could be distorted.

To compensate for this measurement bias, one solution is to separate the plate into four sub-plates, which would have enabled homogenous measurement throughout the cabin. However, this is also difficult to implement, as it would require four sensors and four strictly identical calibrations. So we had to look for a system that was fundamentally simpler to implement and prototype.

2.2 Weighing at the suspension rope

A critical element of the lift is its suspension cables. They must be dimensioned to withstand a weight greater than that recommended in the lift. They are therefore subject to deformation, which it would then be possible to quantify and translate into a usable quantity. Several assemblies have been considered.

2.2.1 Measurement by two electrodes around the cable

Assuming that the lift is held in place by a main suspension cable, on which most of the deformation is exerted, one possible solution would have been to attach two electrodes C_1 and C_2 around the cable and continuously measure the distance l separating them, as shown in figure 1.

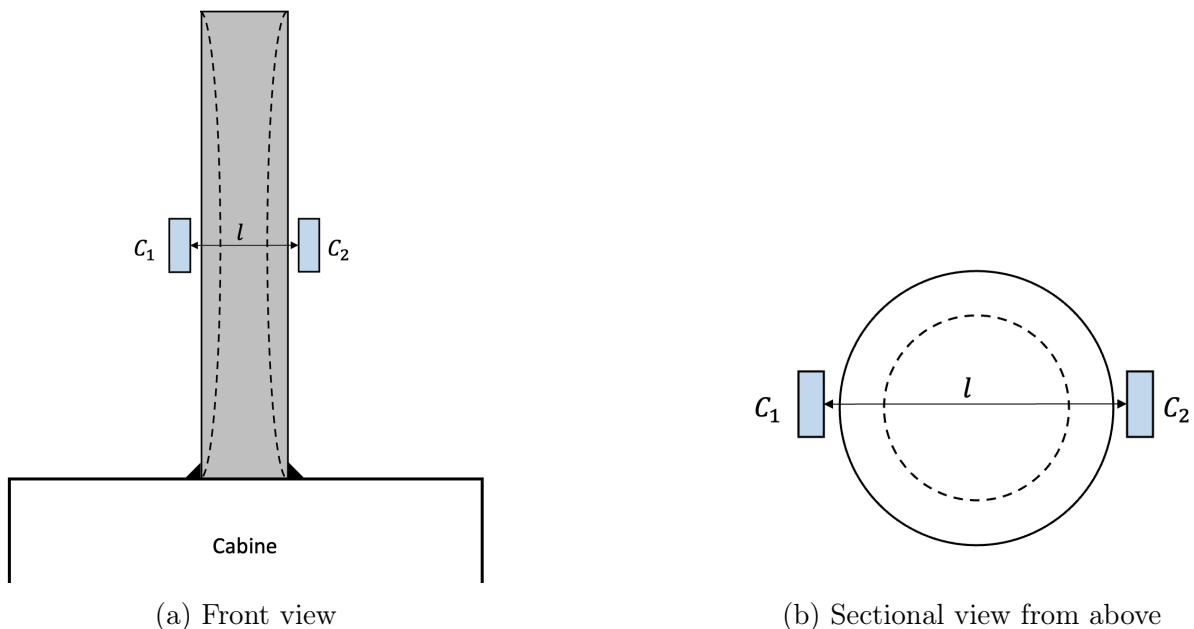


FIGURE 1 – First assembly proposal

In this way, the electrodes generate a different capacitance for each value of l , which can then be related to the weight of the car. The closer the electrodes are to each other, the higher the capacitance value. Although untreated, this approach appears to be reliable and easy to test, for example by replacing the cable with a polymer in order to obtain a greater variation in l .

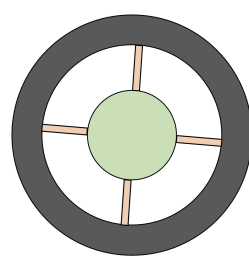
A variation of this set-up would have been to impose a fixed distance between the two electrodes (i.e. to disconnect them from the support cable) and to measure the variation in electric field generated by the deformation of the cable. However, this method requires dielectric properties of the material in tension that could not have been reproduced with a polymer.

2.2.2 Measurement by parallel plane electrodes

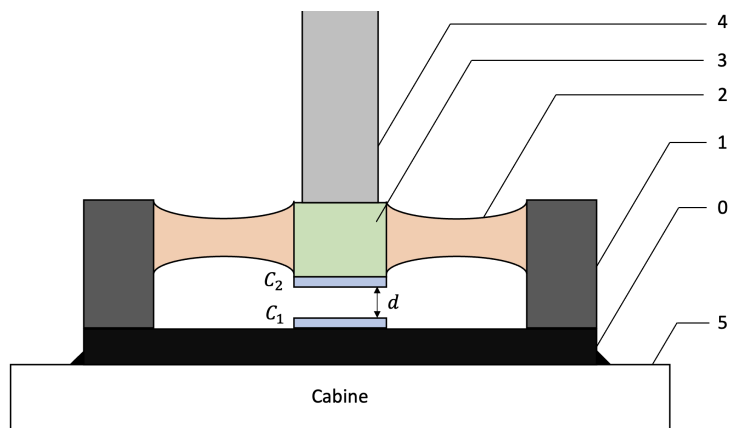
A simple, complete and reproducible approach in the laboratory is to use a load cell between the cabin ceiling and the suspension cable. The force transducer therefore acts as an intermediate part, and is subjected to significant stress. The choice of load cell was made between two options : an S-type load cell and a pancake-type load cell. In the case of the S-type transducer, the force is concentrated at the centre of the loop of the S formed by the part. The strain gauge is then subjected to this deformation and translates it into usable tension. However, such a system is mainly subjected to vertical shear stress. Here, the use of a capacitive sensor is preferred, i.e. one that generates a voltage from a linear displacement. For this reason, the final choice is a pancake-type force transducer [2], which will be suitable for capacitive measurement with a planar capacitor [3].

The sensor built for the proof-of-concept differs from pancake-type load cells on the market. The model designed and studied in this report does not have a strain gauge, but electrodes. It has three parts (see Figure 2) :

- A part integral with the lift ceiling (part 0)
- A circular part 1 attached to 0 and supporting the ribs
- A deformable rib 2 which undergoes the greatest stresses
- A part attached to the suspension cable 3.



(a) Sectional view
from above



(b) Sectional front view

FIGURE 2 – Illustration of the final assembly

The principle of this sensor is based on the translation of part 3 relative to part 0. When a weight is added to the cabin, a return force is applied to the suspension cable, which pulls part 3 upwards. A slight displacement of part 3 is allowed by deforming the ribs 2. Each rib therefore undergoes significant shearing. It is then possible to detect this movement using electrodes C_1 and C_2 . A variation in the distance d modifies the value of the capacitance of the electrodes, which can then be converted into a frequency.

As variations in capacity can generally be detected with a high degree of accuracy, variations in weight will also be detectable, and it is therefore possible to expect high resolution from the sensor. The measurement range is also large, the limiting element being the deformable ribs, as these are the parts most subject to stress and also the most likely to deform plastically or break. The reliability of this sensor is therefore closely linked to the mechanical behaviour of the ribs, which must be deformed within the elastic limit, while avoiding having a system that is too rigid. This raises a problem of dimensioning. The system must be flexible enough to allow sufficient variations in the distance d , but must not exceed the elastic limit of the ribs to avoid creep or breakage.

3 Physical modelling

To understand the system properly, it is worth recalling the sensor's operating principle. When a force F is exerted on the sensor, a distance d is formed between the two electrodes. The capacitance C is then modified, which will also modify the final frequency read by the microcontroller. It is this frequency that will be used as the basis for measuring the force exerted. Obtaining usable measurements therefore depends solely on the deformation of the ribs, which must be dimensioned with the utmost care.

3.1 Sizing ribs

In order to dimension this section, it is essential to use the framework of structural mechanics. All the assumptions necessary for the theory of Euler-Bernoulli beams must be made. The Bernoulli hypothesis is accepted, the cross-section of each rib is assumed to be rectangular, etc. For the design, it is assumed that the beam being studied is in pure shear, as shown in Figure 3. As the design study is carried out on the finished product, the material chosen for the beam is a 6061 aluminium alloy.

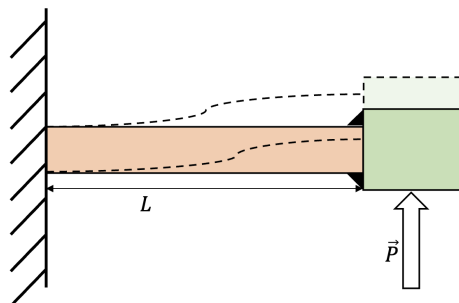


FIGURE 3 – Stress on a beam in pure shear

When a lift is used, perfect safety must be guaranteed, even in the event of overloading. A safety coefficient $s = 5$ is chosen for the bending ribs. This is a typical value for a wire

rope lifting system. The system should therefore not be loaded to more than 20 % of its strength. As the ribs are made of 6061 aluminium alloy, the elastic strength is taken to be $R_e = 470 \text{ MPa}$ [4]. This means that the material can withstand stresses of up to 470 MPa without undergoing permanent deformation.

As the ribs are loaded in shear, it is more appropriate to consider the elastic resistance to sliding R_{eg} rather than the elastic resistance R_e . The latter is defined by the relationship $R_{eg} = 0.5 \cdot R_e$. The value 0.5 is characteristic of aluminium alloys. In addition, to be sure of not entering the plastic domain, the maximum load force is divided by the safety factor. A new term is then introduced : the practical slip resistance R_{pg} , defined by the formula 1.

$$R_{pg} = \frac{R_{eg}}{s} = \frac{0,5 \cdot R_e}{s} \quad (1)$$

Numerically, $R_{pg} = 47 \text{ MPa}$. This is the maximum force allowed on the transducer to maintain good safety. To find the corresponding load in kg, we can calculate the shear stress τ . This is defined by the relationship 2, where T is the maximum tangential force applied to the rib (in this case, the weight of the cabin) and S is the cross-section of the beam to which the force is applied, in this case a rectangular beam with base b and height h .

$$\tau_{max} = \frac{T}{S} \quad (2)$$

In the extreme case considered, the maximum load is therefore the practical sliding resistance R_{pg} and the maximum tangential force is equal to the maximum authorised weight of the cab, $g \cdot m_{max}$. It is therefore possible to write the relationship 3.

$$R_{pg} = \frac{m_{max} \cdot g}{b \cdot h} \quad (3)$$

The maximum mass of the cab is then expressed by the relationship 4.

$$m_{max} = \frac{R_{pg} \cdot b \cdot h}{g} \quad (4)$$

The dimensions of the rib are taken as : *base* = 1 cm, *height* = 3 cm. The mass $m_{max} = 1437.31 \text{ kg}$ is then found. Considering the mass of the lift when empty (between 500 kg and 1500 kg), this value is too low and the authorised limit could be reached if an unfavourable case of use occurs. In this case, the load cell should be fitted with several ribs. Adding a rib distributes the force evenly and therefore doubles the breaking load. For example, with eight ribs, $m_{max} = 11.5 \text{ tons}$, which is a satisfactory result given the high safety factor.

It is also possible to determine the deformation that a stress close to the maximum permissible stress would cause. To do this, it is necessary to make a strong assumption : each beam is now assumed to be in pure bending, as shown in Figure 4 ; the beam is subjected to a force (in this case a weight P) exerted at a point located at a distance L from the base of the rib.

This is a strong assumption because it neglects the shear that the beam undergoes. However, it allows us to write the formula for the deflection generated according to the

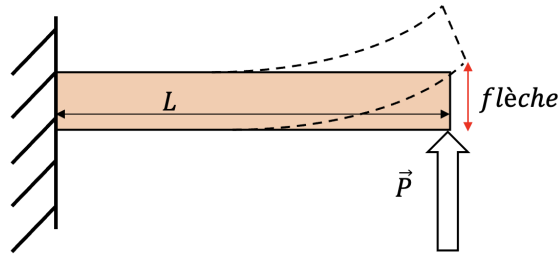


FIGURE 4 – Stress on a beam in pure bending

weight P applied (5). L is the length of the beam, E is the Young's modulus in bending of the material, and I is its squared moment.

$$fleche = \frac{PL^3}{3EI} \quad (5)$$

The quadratic moment I is defined by the expression 6, where b is the width of the beam and h its height. This expression is specific to a beam with a rectangular cross-section.

$$I = \frac{bh}{12} (b^2 + h^2) \quad (6)$$

For the dimensions of the ribs chosen above, $I = 2.5 \cdot 10^{-8} m^4$. For an aluminium alloy rib (length $L = 4$ cm), the Young's modulus E is approximately 58 GPa. This gives a deflection of 207 μm . If the transducer is fitted with 8 ribs, the force is distributed evenly over each rib, giving a maximum permissible deflection of 26 μm . The maximum permissible deflection of the transducer is therefore low, so the challenge is to have a transducer that is sufficiently accurate to distinguish between variations in capacity generated by such small displacements.

So, when sizing the capacitive force transducer, it is essential to choose the right materials to ensure that it works properly. Considering a housing and ribs made of aluminium alloy (a common and inexpensive material), a crucial factor is the number of ribs the system has, as each rib added improves the system's strength. However, adding too many ribs would make the system too rigid and affect its resolution. A direct solution would be to reduce the number of ribs or to reduce the safety factor, which is not satisfactory, because the maximum load would decrease and the risk would increase. However, as the deflection varies according to the cube of the length L of each rib, the most effective solution is to increase this value : this does not affect the elastic limit of the system, but only the value of the deflection. The sensor is therefore very flexible : it is possible to adjust the parameters to maximise the deflection or not, depending on the accuracy of the capacity measurements.

3.2 Mathematical modelling

To express the output (frequency) as a function of the input (mass), it is necessary to translate the mass into capacitance, then the capacitance into frequency. To do this, the equations 6 and 7 are used to establish the distance between the electrodes according to

the weight of the cab. This distance is equal to the distance in neutral conditions d_0 (no weight on the sensor) added to the deflection generated by the weight of the cab. As the force is divided by the number of ribs n available to the loadcell, it is essential to divide the deflection by n . The formula 7 therefore translates the mass m of the cab into the distance d between the electrodes. It is then possible to quantify the deflection, i.e. the deflection obtained for an applied force equal to 10kgf. This is 69 μm .

$$d = d_0 + \frac{9,81L^3}{3EIn} \cdot m \quad (7)$$

To translate these variations in distance into variations in capacitance, the formula for the planar capacitor [5] is very appropriate. Since the two electrodes are assumed to be plane, parallel and infinite, the chosen arrangement can be likened to a plane capacitor, and the relationship 8 can therefore be written. ϵ_0 is the permittivity of vacuum, ϵ_r is the permittivity of air (taken at 1 F/m), S is the surface area of an electrode and d is the distance between the electrodes, given by the formula 7 previously found.

$$C = \frac{\epsilon_0 \epsilon_r S}{d} \quad (8)$$

The capacitance is translated into frequency by means of a formula found experimentally, using the procedure described in section 4.1. The formula is as follows :

$$C = \frac{4.10^{-7}}{f - 5111,1} \quad (9)$$

It is then possible to describe the output of the sensor as a function of the input using the equation 10. The frequency therefore evolves in an affine manner with the mass of the cabin. In particular, it is possible to obtain the sensitivity of the sensor directly by developing this expression. By calculating it, the result obtained is 159.7 Hz/kgf.

$$f = 5111,1 + \frac{4.10^{-7}}{\epsilon_0 \epsilon_r S} \left(d_0 + \frac{9,81L^3}{3EIn} \cdot m \right) \quad (10)$$

$$S = \frac{3,92 \cdot 10^{-6} \cdot L^3}{3EIS \epsilon_r \epsilon_0 n} \quad (11)$$

3.3 3D modelling

Two 3D models of the sensor were produced using two different software packages : Fusion360 and Comsol. The first modelling in Fusion360 is carried out by revolution of the plane shown in figure 5. The numerical values chosen are as follows :

- Rib width $b = 2$ mm
- Rib height $h = 24$ mm
- Rib length $L = 4$ cm
- Young's modulus $E = 3.25$ GPa
- No-load distance between electrodes $d_0 = 1$ mm
- Number of ribs $n = 4$
- Electrode diameters $diam = 5$ cm

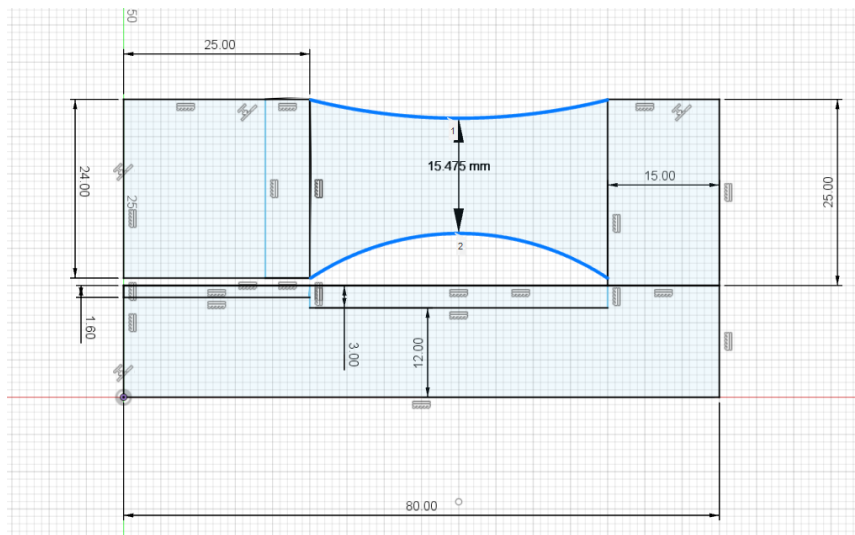


FIGURE 5 – Cross-section of the model seen from the front revolution

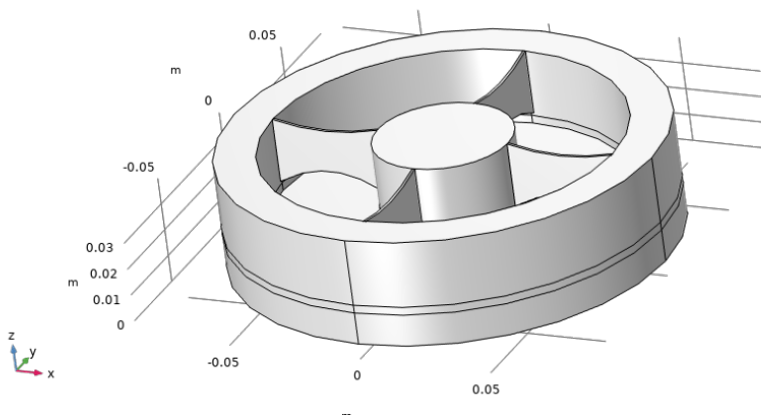


FIGURE 6 – 3D model in COMSOL

A simulation with a cabin weight of 100 N is carried out, the results of which are shown in figures 7 and 8. These figures also show the stress distribution on the object. It can be seen that these are concentrated on the ribs, which is how it should work. It is also possible to read the deflection values (Figure 9). The deflection obtained on Fusion360 is 148 μm , and 80 μm on Comsol. It can be seen that the result obtained on Comsol is closer to that obtained by mathematical modelling (69 μm).

Comsol also has a multiphysics coupling that allows the capacitance C to be approximated as a function of the force applied. It is then possible to translate the capacitance into frequency using the formula 9 and plot the transducer output (Hz) against the input (kgf). This reveals perfect linearity and a sensor sensitivity of 184.4 Hz/kgf. It can then be seen that this value is very close to that found by the mathematical model (159.7 Hz/kgf). The mathematical and 3D modelling therefore seem to indicate that the sensor's deflection is close to 70 μm and its sensitivity close to 160 Hz/kgf. It is now time to check experimentally whether these values are realistic.

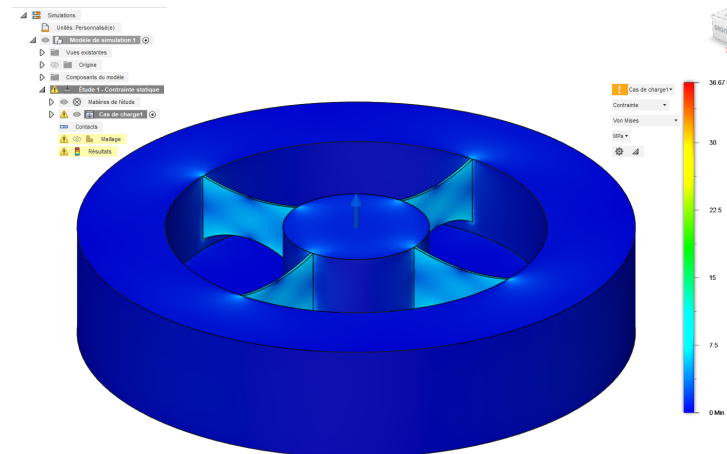


FIGURE 7 – Fusion360 3D model - stress distribution

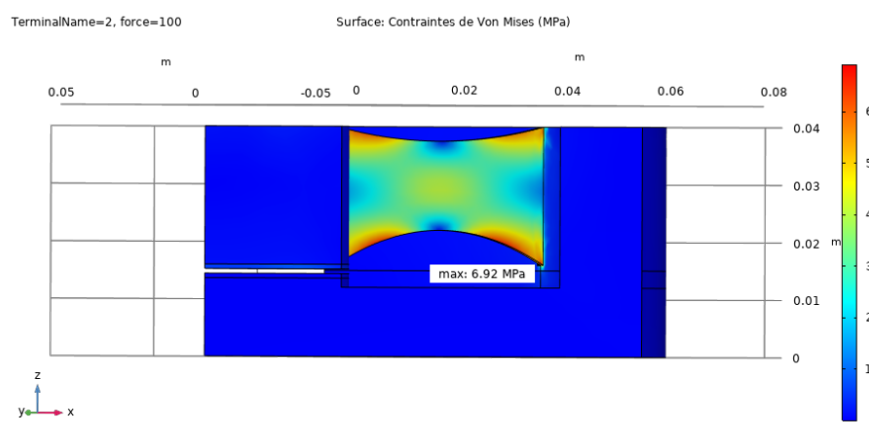


FIGURE 8 – COMSOL 3D model - stress distribution on a rib

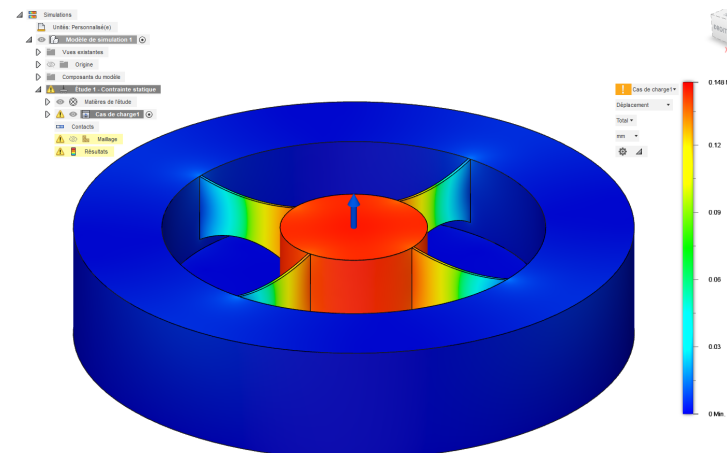


FIGURE 9 – Deformation distribution - 3D simulation

4 Experimental results

In order to obtain usable experimental results, we need to design a prototype and a conditioning circuit capable of translating the electrode capacitance into a frequency. For the prototyping of this capacitive force sensor, the choice was made to work with polylactic acid (PLA) so that it could be built using 3D printing. A first prototype was built and fitted with a hook in the centre of the underside, enabling a mass to be attached. A second prototype ("v2") was also built, but differed from the first in that the underside was denser and the attachment points for the mass were evenly distributed across the surface.

4.1 Conditioner circuit design

The main challenge for this sensor is to make the variation in capacitance readable by a microcontroller. This section therefore highlights the various stages required to manufacture a suitable conditioner circuit.

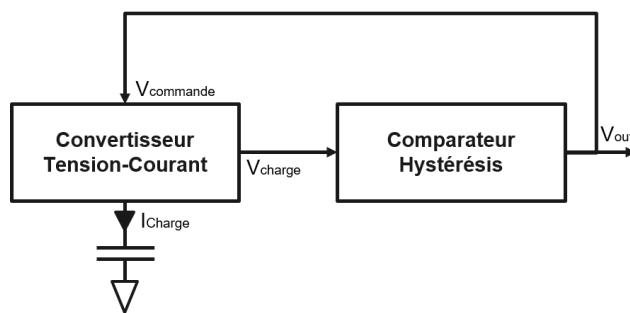


FIGURE 10 – Conditioner block diagram

The conditioner circuit is based on the charging time of a capacitor. This choice is motivated by the desire to obtain a direct link between the oscillation frequency of the circuit and the value of the capacitor, without having to worry about the amplitude fluctuation of the voltage across the capacitor. The conditioner therefore consists of a current-to-voltage converter connected to the variable capacitor, which leads to a hysteresis comparator looped back to the control voltage.

Voltage-to-current converter

The first step in creating the conditioner is to create the voltage-to-current converter. This regulates a constant load current on the capacitor, controlled by a DC voltage. An operational amplifier can be used to easily create a current-to-voltage converter, making it easier to measure the intensity of a current in an electrical circuit.

The amplifier will be considered ideal during the study, which means that $V_- = V_+$. In addition, the input resistances and impedance of the operational amplifier are very high, which means that the current drawn can be kept to a minimum.

$$V_- = \frac{\frac{V_{out}}{R_1}}{\frac{1}{R_1} + \frac{1}{R_2}} \quad (12)$$

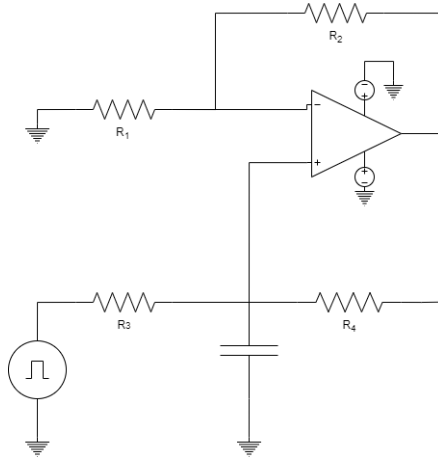


FIGURE 11 – Electrical diagram voltage current converter

However $R_1 = R_2 = 1 \text{ M}\Omega$

$$V_- = \frac{V_{out}}{2} \quad (13)$$

$$V_+ = \frac{\frac{V_{out}}{R_3} + \frac{V_{in}}{R_4}}{\frac{1}{R_3} + \frac{1}{R_4} + jC\omega} \quad (14)$$

And $R_3 = R_4 = 5\text{M}\Omega$

$$V_+ = \frac{V_{out} + V_{in}}{2 + jR_3C\omega} \quad (15)$$

Combining with 13 :

$$V_+ = \frac{V_{in}}{jR_3C\omega} \quad (16)$$

According to Ohm's law : $i_c = V_+ + jC\omega$ hence :

$$i_c = \frac{V_{in}}{R_3} \quad (17)$$

This formula shows the link between the input voltage and the current flowing through the capacitor. The current is therefore dependent on the input voltage.

Simulation

The capacitance is set at $C = 10 \text{ pF}$ for the simulations. The curves shown in Figure 12 were obtained :

The input voltage is a square-wave signal varying from -5 V to 5 V every 10 μs . According to Ohm's law for a capacitor, $i_c = \frac{\Delta V}{\Delta T}$.

In the case where $V_{in} = 5 \text{ V}$, the voltage at the edge of the capacitor increases gradually until it reaches a value of $\Delta V = \frac{V_{in}}{R_3C\omega}\Delta T$ with $\Delta T = 10 \mu\text{s}$, i.e. $\Delta V = 1 \text{ V}$. Similarly, when $V_{in} = -5 \text{ V}$, the voltage at the edge of the capacitor decreases progressively until it reaches a value of $\Delta V = -1 \text{ V}$.

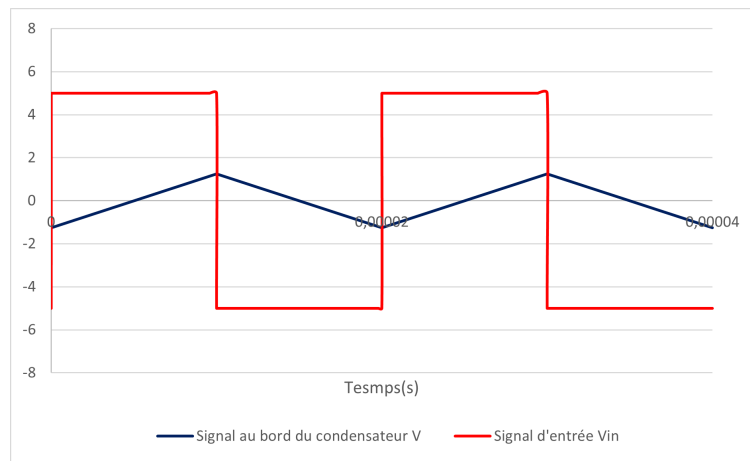


FIGURE 12 – Voltage-to-current converter simulation

Hysteresis comparator

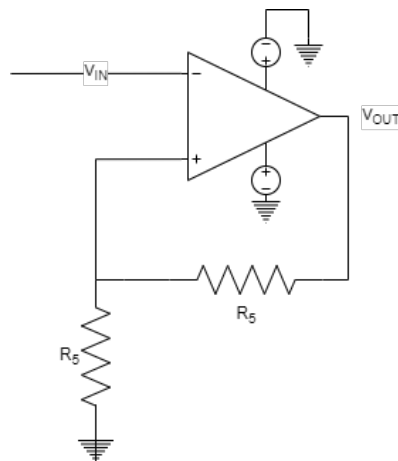


FIGURE 13 – Electrical diagram of hysteresis comparator

Looping is done on V_+ , so $V_+ > V_-$ si $V_{out} = 5$ V and $V_+ < V_-$ si $V_{out} = -5$ V. This amounts to having $V_{out} = 5$ V when $V_{in} > V_{out} \frac{R_6}{R_6 + R_5}$, hence $V_{in} > 1,25$ V and by analogy, $V_{out} = -5$ V when $V_{in} < 1,25$ V.

Simulation

The input voltage is a square-wave signal varying from -2 V to 2 V every 10 μ s. The simulation results are shown in Figure 14. The expected result is obtained.

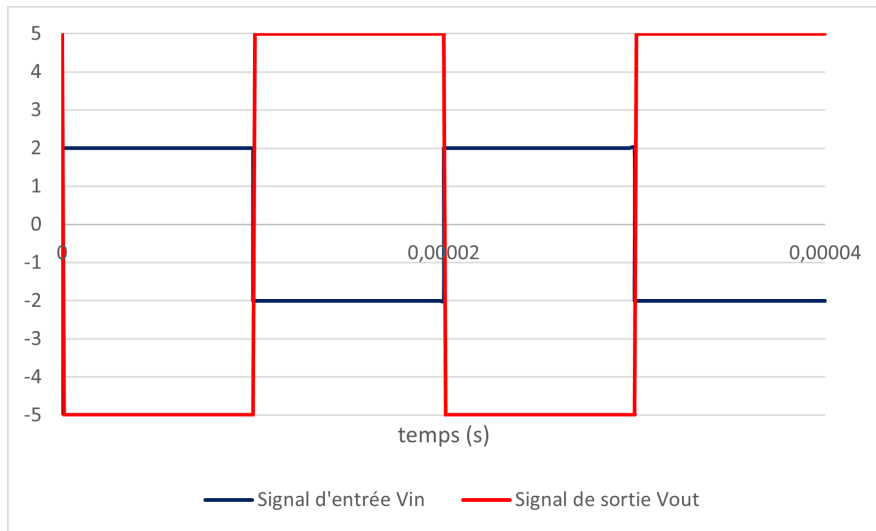


FIGURE 14 – Hysteresis comparator simulation

Looping

The two circuits described above are now interconnected. The voltage across the variable capacitor influences the switching of the hysteresis comparator.

The capacitor charges more slowly when its value is higher than that of a smaller capacitor. When the voltage across the capacitor reaches the switchover threshold, the comparator switches and the output voltage is applied to the capacitor. The capacitor then discharges when its voltage exceeds a value proportional to the comparator's switching threshold, creating an oscillation in the voltage across the capacitor between two values.

The frequency of oscillation, which depends directly on the value of the capacitor, is inversely proportional to the time taken to charge and discharge the capacitor. The aim of the system is to enable the microcontroller to control the oscillation frequency as a function of the variation in capacitance.

Furthermore, in normal operation, the power supply delivered by the microcontroller is not symmetrical, but from 0 to 5V. So a 5V power supply is added, followed by a voltage divider bridge as shown in the diagram below :

Simulation

A simulation is carried out using $C = 5\text{pF}$, then $C = 7.5\text{pF}$ and finally $C = 10\text{pF}$.

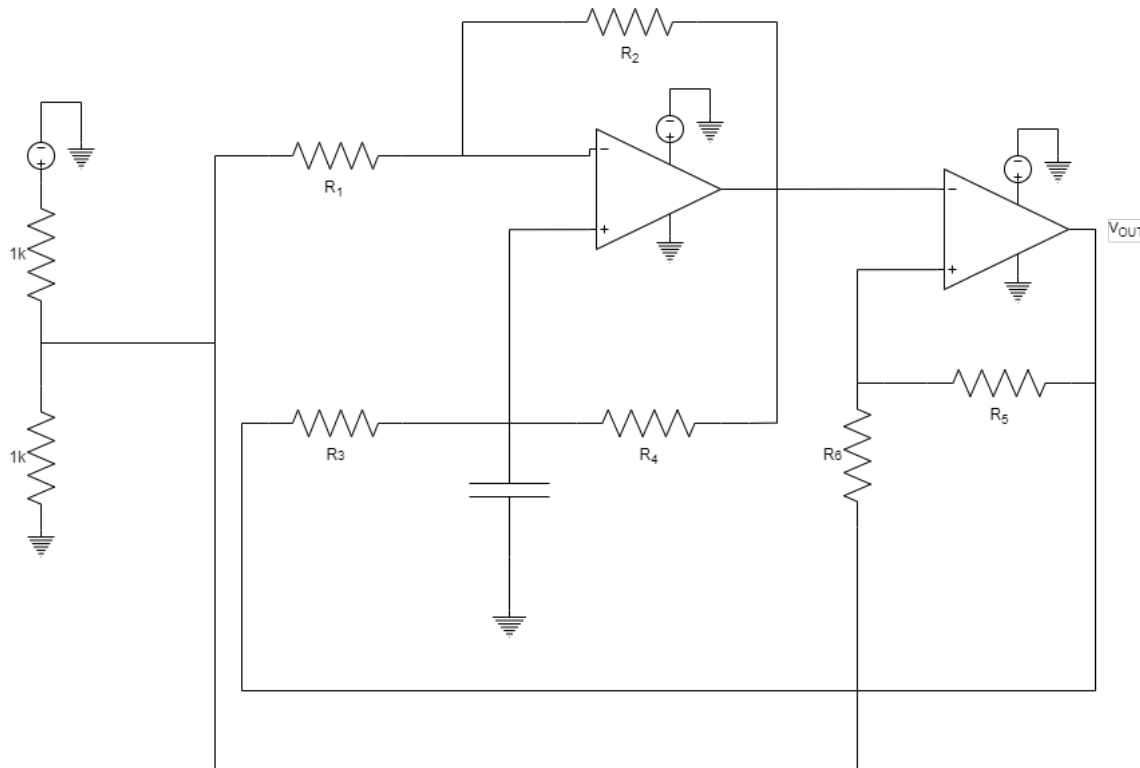


FIGURE 15 – Converter simulation

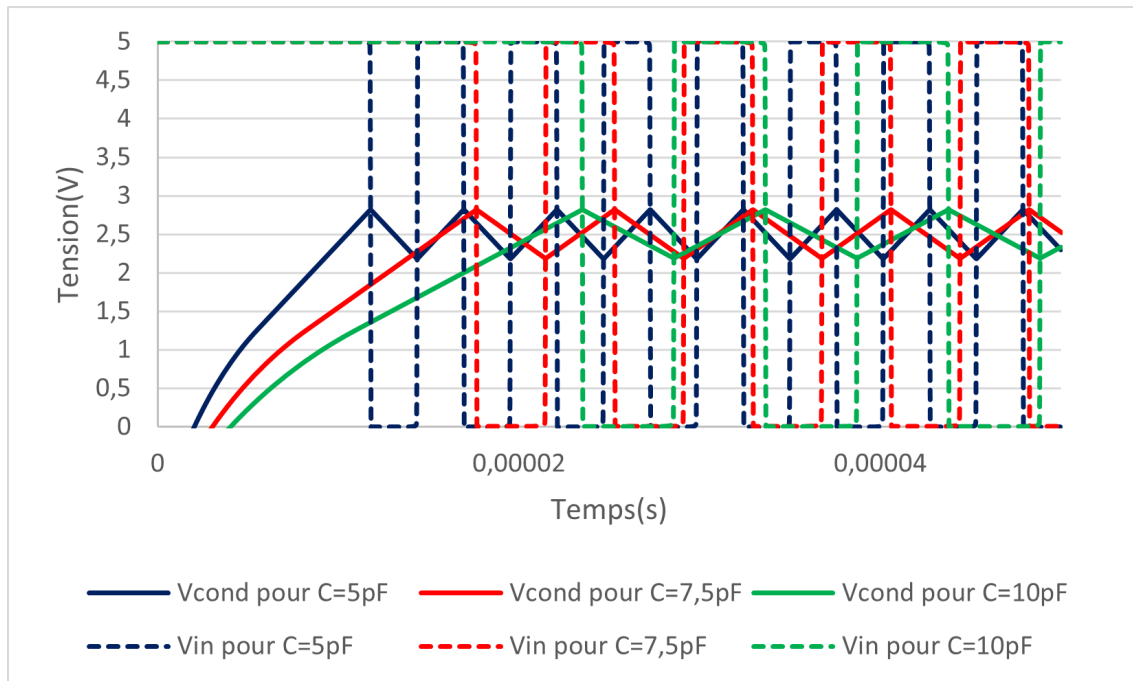


FIGURE 16 – Converter simulation

In the figure, the charge voltage of the 5 pF capacitor is shown in blue, with the corresponding flip-flops. In green, on the other hand, we can see the charging voltage of the 10 pF capacitor with its flip-flops, for an identical charging current. It can be seen that the charge voltage of the 5 pF capacitor varies more than that of the 10 pF capacitor over

a given period of time. As a result, the 5 pF capacitor charges and discharges faster than the 10 pF capacitor. The impact of this load difference on switching is directly observed : the 5 pF capacitor switches more often over a given period of time, because it reaches the switching thresholds more quickly than the 10 pF capacitor. The frequency of oscillation can therefore be related to the value of the capacitor.

$$|i_c| = \frac{V_{in}}{R_3} = C * |\Delta V| * F \quad (18)$$

But $|\Delta V| = \frac{V_{in}}{2}$, hence :

$$F = \frac{2}{C * R_3} \quad (19)$$

The resistors of the hysteresis comparator are modified to obtain : $\frac{R_5}{R_5+R_6} = \frac{1}{2}$. The previous result is then :

$$F = \frac{1}{C * R_3} \quad (20)$$

Experimental law of behaviour

In reality, metallic components generate a parasitic capacitance that disturbs the linear relationship between frequency and capacitance. To determine the equation for this parasitic capacitance, three frequency measurements were carried out with capacitances of 10 pF, 100 nF and 200 nF :

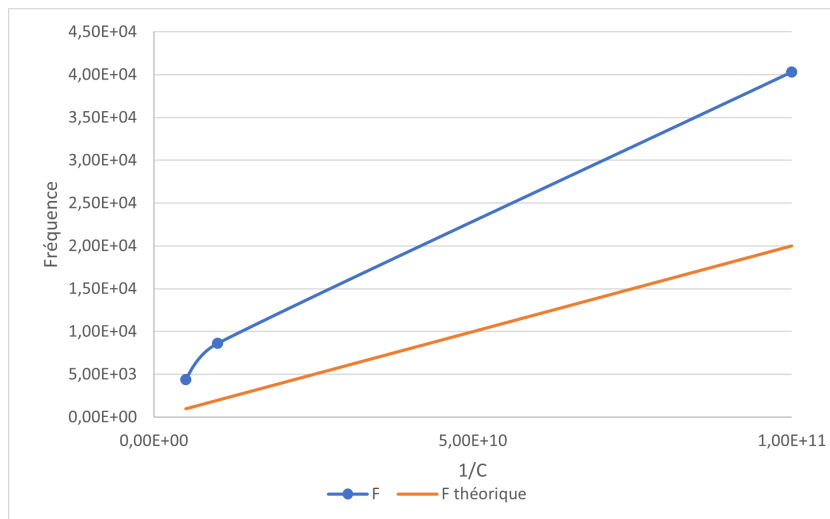


FIGURE 17 – Frequency reading according to $1/C$

Metal components, the quality of soldering and electromagnetic interference create a slight difference between the theoretical frequency and the experimental frequency.

The parasitic capacitance is close to 10 nF, which may explain the non-linearity between $C = 10$ nF and $C = 100$ nF. Therefore, for simplicity, the frequency of the capacitor $C = 10$ nF has been neglected.

Experimental measurement of the frequency gives the following equation :

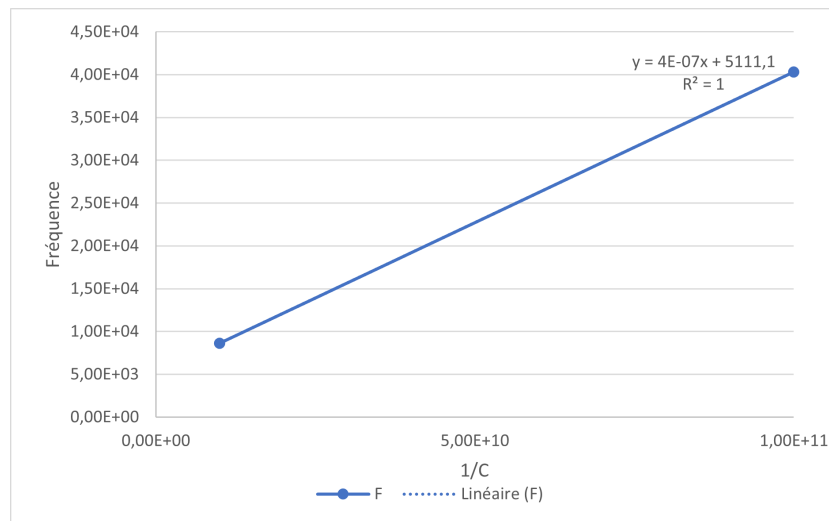


FIGURE 18 – Frequency equation according to $1/C$

$$C = \frac{4 \cdot 10^{-7}}{f - 5111,1} \quad (21)$$

4.2 Tensile test

First prototype

The first prototype was built and subjected to a tensile test with a Mark-10 machine at a force of 0 to 100 N. A photo of the experimental set-up is shown in Figure 1. The test was carried out on a load cycle from 0 to 100 N and then a discharge cycle from 100 to 0 N, in 10 N iterations. The graph of the frequency obtained as a function of the force applied is given in Figure 19.

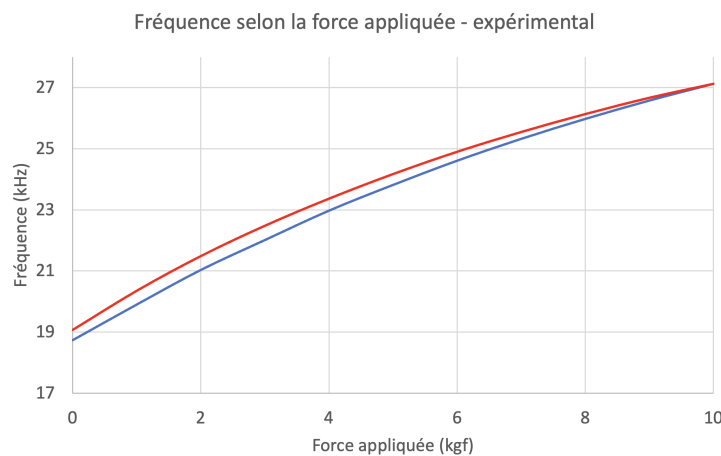


FIGURE 19 – Frequency as a function of force - experimentation

This tensile test provides a great deal of information about the sensor. First of all, it is possible to observe the appearance of hysteresis, i.e. the sensor is slightly deformed when



FIGURE 20 – Experimental tensile test set-up

subjected to a force of 100 N. As this deformation is elastic and not plastic, it returns to its initial shape after a certain period of time. The frequency does not change linearly with the force applied, unlike the results calculated previously. In addition, the frequency variation is significantly greater than in the calculated model. The numerical performance values of the sensor are summarised in Figure 21.

Sensitivity	834,1 Hz/kgf
Maximum linearity error	8,8 % \iff 738,4 Hz/kgf
Maximum hysteresis error	5,8 % \iff 486,7 Hz/kgf
Maximum combined error	13,2 % \iff 1107,6 Hz/kgf
No-load distance	0,59 mm
Empty distance deviation from model	0,41 mm
Deflection	360 μ m
Deflection deviation from model	295 μ m

FIGURE 21 – Prototype performance

It therefore appears that the first prototype is far too flexible compared with the mathematical model and the Comsol model. One of the critical uncertainties here is the actual empty distance between the d_0 electrodes, which is difficult to know precisely. Indeed, during 3D printing, it is possible that filaments are deposited on the construction and modify the distance between the electrodes. However, d_0 has no influence on the sensitivity of the sensor, as shown by the equation 11. In fact, the only parameters affecting sensitivity are :

- The length of the rib L , which cannot be increased because it is a rigorously verified constant.
- Young's modulus E . This value is taken to be 3.25 GPa, but may vary depending on the conditions (prototype printing speed, fill factor, temperature, etc.). It is possible that the actual value will be different. However, by taking $E = 3$ GPa, the sensitivity only increases to 166.2 Hz/kgf, which is still too far from the experimental sensitivity (834.1 Hz/kgf).
- The quadratic moment I , which is constant and calculated from the precise dimensions of each rib.

- The number of ribs n , the permittivity of vacuum ϵ_0 and the permittivity of air ϵ_r , which are immutable constants.
- The surface of the electrode S . The actual diameter may differ very slightly from 5 cm, but this has very little influence on the model.

It therefore appears that the model as a whole cannot be modified. This discrepancy between the model and reality can have two sources :

1. A model that is fundamentally too rigid. It cannot be ruled out that the assumptions made to work within the framework of structural mechanics are too strong for this use case.
2. Too flexible a prototype. It is possible that the prototype was made too lightly, and that undesirable deformations appeared in various places on the object.

Second prototype

The same tests were carried out under conditions as similar as possible with the second prototype equipped with three attachment points distributed over the underside. The graph of the frequency read as a function of the force applied is given in figure 22. Several improvements over the first prototype can be seen, such as a reduction in hysteresis and a decrease in sensitivity, in line with the model. The results are summarised in Table 23.

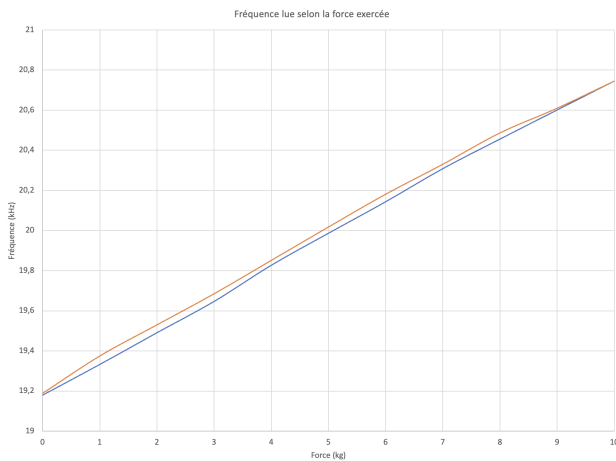


FIGURE 22 – Experimental results for the second prototype

Sensitivity	158,5 Hz/kgf
Maximum linearity error	2,15 % \iff 33,59 Hz
Maximum hysteresis error	4,98 % \iff 77,86 Hz
Maximum combined error	5,05 % \iff 78,99 Hz
No-load distance	0,64 mm
Maximum deflection	70,8 μ m
Deflection deviation from model	1,37 μ m
Maximum error of measurement	500 gf
Resolution	< 500 gf

FIGURE 23 – Prototype v2 performance

4.3 Creep test

It has been observed that the sensor has a viable operating principle, in that its resolution is compatible with the use of a lift. On the other hand, there is a question mark over the sensor's lifespan. It is destined to be in constant use, i.e. when the lift is empty, the sensor still supports the weight of the cabin, which remains considerable. It is therefore reasonable to assume that the sensor is likely to undergo slight, continuous deformation (creep). One experimental method of checking whether the sensor behaves in this way is to keep the sensor subjected to a constant force and observe whether the frequency varies. If it does, then the transducer is likely to have a reduced lifetime and increasingly inaccurate measurements over time.

In the case of the v1 prototype, a significant hysteresis phenomenon was observed, i.e. the transducer deformed after withstanding a force of 10 kgf. To quantify this creep more precisely, the sensor can be placed under continuous load and the frequency read regularly recorded. Once this frequency has been converted into distance, it is possible to plot the sensor's deflection as a function of time, as shown in Figure 24.

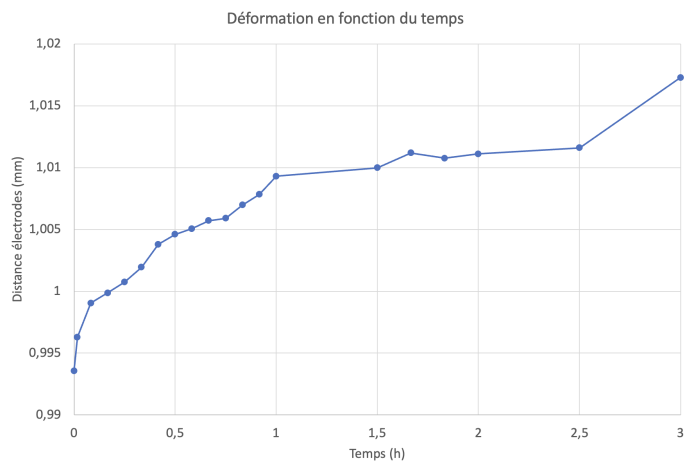


FIGURE 24 – Distance between electrodes over time (prototype v1)

The graph obtained is typical of the deformation of a part made of [6] polymer. It has three distinct parts :

1. A stabilisation zone, in the first hour
2. A linear creep zone, between 1h and 2h30
3. A zone of rapid acceleration, occurring just before polymer rupture

It can therefore be argued that if the experiment had been extended any longer, the polymer would have failed and the prototype would have been destroyed. What's more, the total deformation observed in three hours is 23.7 µm, which is a widely detectable variation.

The same test was carried out with the second prototype. By taking only the deflection into account, it is possible to directly compare the creep of the two prototypes (Figure 25). A clear difference in deflection can be observed between the two prototypes. Indeed,

after 7 hours of loading, the v2 prototype does not seem to have reached, or has barely reached, the linear creep phase. By extension, the lifespan of prototype v2 appears to be much greater than that of prototype v1.

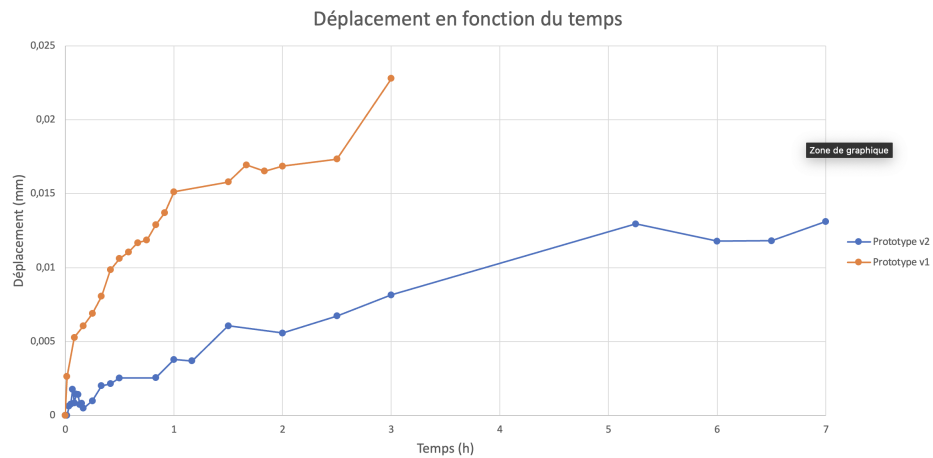


FIGURE 25 – Deflection of prototypes at 10 kg load

4.4 Relaxation test

In the same way, it is possible to investigate the relaxation time of the sensor, i.e. the time required to return to the initial position. The experimental protocol is also similar : with no load, the frequency given by the sensor after being solicited for a prolonged period is tracked over time and then converted into distance. The result is the graph shown in Figure 26.

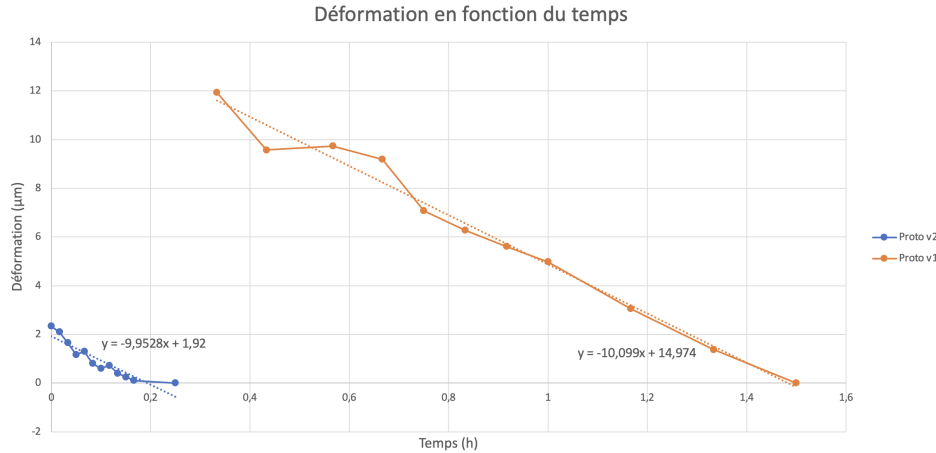


FIGURE 26 – Sensor relaxation time after 3 hours of use

Overall linear relaxation can therefore be observed for both prototypes. It is also interesting to note that the relaxation speed is fairly similar for the two prototypes ($10.1 \mu\text{m}/\text{h}$ for the v1 prototype and $10.0 \mu\text{m}/\text{h}$ for the v2). The relaxation rate is therefore independent of the sensor geometry and its hysteresis.

5 Analysis of results

In order to visually compare all the models and prototypes, it is possible to display the plot of frequency versus force for each model and prototype. The result is shown in figure 27. As expected, the v1 prototype is much more sensitive than the other models and is not relevant to this study. On the other hand, the mathematical model calculated using beam theory seems to corroborate the Comsol model and the experimental results of the v2 prototype.

By discarding the v1 prototype and adjusting the mathematical model to the real no-load distance d_0 , it is possible to obtain the graph 28. In fact, the no-load distance is an uncertainty linked to uncontrollable parameters : the mathematical model needs to be adjusted to the real no-load distance (less than 1 mm), obtained by converting the no-load frequency. The results are very convincing : the models match reality very well and the different sensitivities are very close. It is therefore possible to state that in the case of low loads and low displacements, structural mechanics and beam theory are in good agreement with electrostatics, despite assumptions which, at first sight, may seem very strong. However, this statement needs to be qualified by considering heavier loads and a much wider measurement range ; in this case, even the slightest difference in sensitivity between the model and reality can lead to false measurements. In this case,

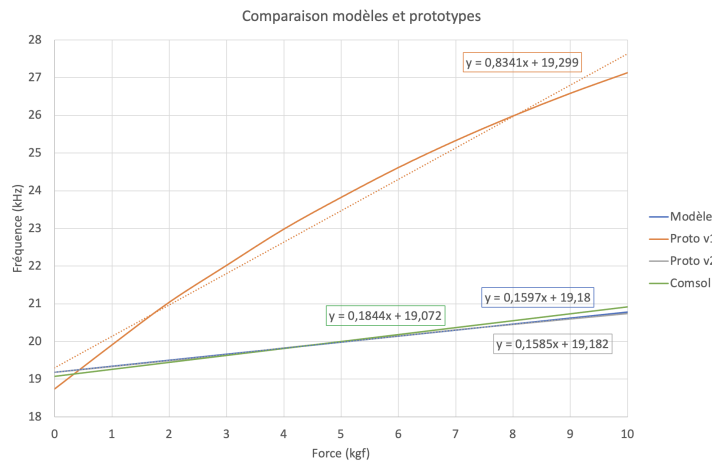


FIGURE 27 – Comparison of the Comsol mathematical model and the two prototypes

even the slightest difference in sensitivity between the model and reality can lead to false measurements, and more rigorous modelling is required to remedy the situation.

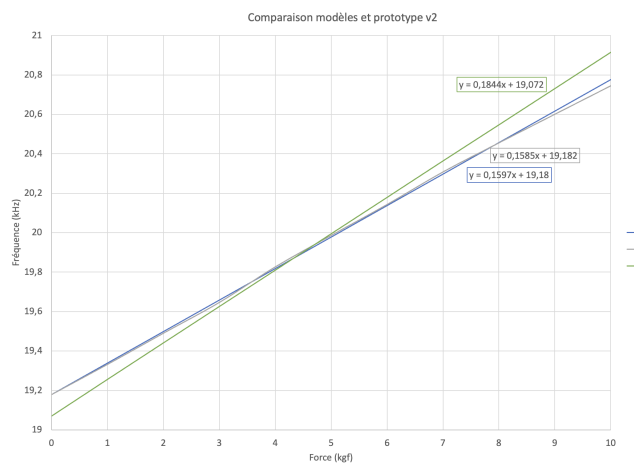


FIGURE 28 – Comparison of models and prototype v2

The notable results are summarised in the table below :

	Model	Comsol	Prototype v2	Prototype v1	Fusion360
Sensitivity (Hz/kgf)	159,7	184,4	158,5	834,1	-
Deflexion (μm)	69	80	68	360	148

6 Improvement ideas

Many improvements can be considered to make the system more robust and compact. In particular, unfavourable situations in which the system could give false measurements should be considered. In particular, if one of the ribs breaks due to fatigue, there is a risk that electrode C_1 will no longer be parallel to electrode C_2 , as shown in figure 29.

This situation presents two risks : an inaccurate weight measurement and an increased risk of breakage. To prevent the cab from falling, adding safety cables in several places is a

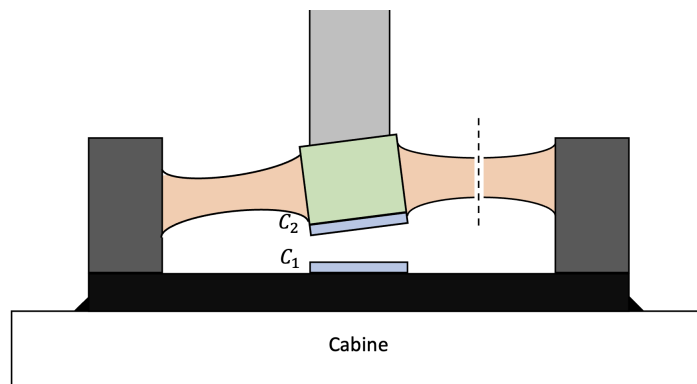


FIGURE 29 – Non-parallel electrodes in the event of a rib fracture

simple and viable solution. The length of these cables should be slightly greater than that of the suspension cable, so that they are not subject to stress under normal circumstances. As far as the risk of falsified measurements is concerned, it is difficult to guarantee that the electrodes are perfectly parallel at all times : the entire sensor will probably have to be replaced if a rib breaks, or the calibration will have to be redone.

Although the system is meticulously dimensioned for the context in which it will be used, it is not impossible to imagine a miniaturised version, designed to measure smaller weights, for example for a luggage scale. The factor to be reduced would then be the surface area of the electrodes. However, the formula 8 reminds us that reducing the surface area of the electrodes also reduces the capacitance. However, it would be difficult to quantify the variation of a capacitance that is too small. One solution is to change the relative permittivity factor of the medium between the ϵ_r electrodes. For example, by immersing this medium in glycerol, with an electrical permittivity of $\epsilon_r \approx 42 \text{ F.m}^{-1}$, it is possible to multiply the capacitance by about 42. Figure 30 shows such a use case, with glycerol shown in red. The surface area of the electrode can therefore be reduced considerably without the capacitance becoming too low. The major disadvantage of this method is the essential addition of a "cover" part (marked 6 in Figure 30), sealed with part 1, thus preventing the fluid from overflowing. Sealing between parts 0 and 1 is also necessary. If this solution is adopted, special precautions should be taken with regard to the ageing of the submerged ribs and the possible evaporation of glycerol, which could damage the system.

There are undoubtedly many other improvements that can be made to the system, and the above is not an exhaustive list.

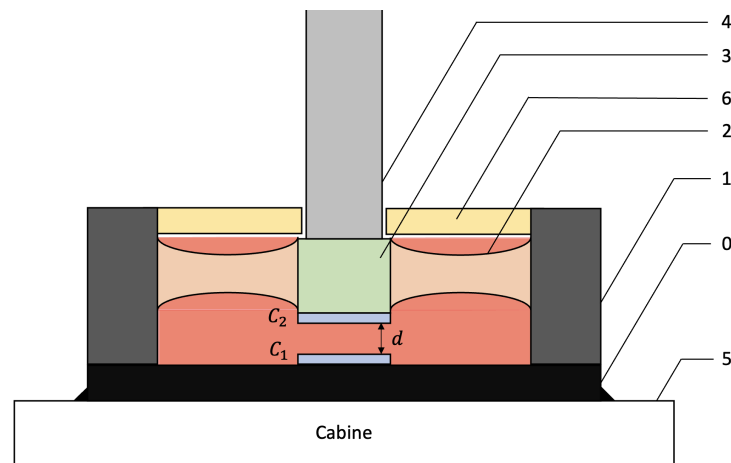


FIGURE 30 – Submerged capacitor

7 Synthesis

The design of a capacitive force transducer therefore required a structural mechanics approach in order to obtain a mathematical model that was faithful to reality. In particular, it appears that it is possible to produce a capacitive force sensor with largely satisfactory performance in the context of a lift cabin weighing application. Indeed, for a prototype with a small measurement scale, the specifications seem to have been met : a maximum measurement error of 500 g, a resolution of less than 500 g, and a sensitivity very close to the mathematical model. The only limitation seems to be the lifetime of the sensor, which risks permanent creep as it supports the cab. However, this risk can be avoided by careful selection of the sensor material and careful dimensioning of the ribs. It is therefore possible to answer in the affirmative the question of choosing a capacitive sensor to measure the weight in a lift car.

Références

- [1] Zhang YANBIN et al. « The Statistics And Analysis Of Annual Fault Repair Report Of An Elevator Company ». In : *2020 2nd International Conference on Machine Learning, Big Data and Business Intelligence (MLDBI)*. 2020, p. 576-579. DOI : [10.1109/MLDBI51377.2020.00121](https://doi.org/10.1109/MLDBI51377.2020.00121).
- [2] Vijay KAMBLE, Vasudev SHINDE et Jayant KITTUR. « Review on optimization of load cells ». In : (oct. 2021).
- [3] X. HU et W. YANG. « Planar capacitive sensors – designs and applications ». In : *Sensor Review* 30 (2010), p. 24-39. DOI : <https://doi.org/10.1108/02602281011010772>.
- [4] Andrew COLE. « AL 6061-T6 Aluminium Alloy Properties, Tensile and Yield Strength, Thermal Conductivity, Modulus of Elasticity, Equivalent Material ». In : *The World Material* (2020).
- [5] Dan Mihai řTEFĂNESCU. « Handbook of Force Transducers : Principles and Components ». In : (20011).
- [6] J. Sweeney I. M. WARD. « The Mechanical Properties of Solid Polymers ». In : (2004).